Scaling state of dry two-dimensional froths: Universal angle-deviations and structure

Andrew D. Rutenberg* and Micah B. McCurdy
Department of Physics and Atmospheric Science, Dalhousie University, Halifax, Nova Scotia, Canada B3H 3J5
(Received 10 February 2005; published 13 January 2006)

We characterize the late-time scaling state of dry, coarsening, two-dimensional froths using a detailed force-based dynamical model. We find that the slow evolution of bubbles leads to small and decreasing deviations from 120° angles at threefold vertices in the froth, but with a side-number dependence that is independent of time and apparently universal. We also find that a significant number of $T1$ side-switching processes occur for macroscopic bubbles in the scaling state, though most bubble annihilations involve four-sided bubbles at microscopic scales.

DOI: 10.1103/PhysRevE.73.011403 PACS number(s): 82.70.Rr, 68.90.+g, 05.70.Ln, 05.10.−a

I. INTRODUCTION

Froth systems have a distinctive, close-packed cellular structure of bubbles that are bounded by smoothly curving walls (films) that intersect in pointlike Plateau borders (vertices). Random soap froths continually coarsen due to gas diffusion between individual bubbles [1]. Eventually, these dynamic froths exhibit a characteristic length scale that grows as a power law in time, $L \sim t^{1/2}$, as well as a time-independent "scaling" structure. This scaling state, or regime, of froths is observed experimentally in both two-dimensional (2D) [2] and three-dimensional (3D) froths [3]. Our understanding of the scaling state of 2D soap froths is largely built on the foundation of experimental [4,5] and computational [6–10] studies of 2D froths in the dry-froth limit with Plateau borders of vanishing size.

In the dry-froth limit, and under the approximation that bubble-wall curvatures and intersection angles exactly satisfy local force balance, individual bubble areas evolve with von Neumann's law,

$$dA_n/dt = \pi\sigma D(n-6)/3, \tag{1}$$

where A_n is the area of a bubble with n sides, σ is the surface tension of the films, and D is the coefficient of diffusion of gas between adjacent bubbles [11]. This slow, continuous evolution is supplemented with dynamical rules for fast, topological rearrangements: both "$T2_n$" processes of bubble annihilation for n-sided bubbles, and "$T1$" side-swapping processes between adjacent bubbles (see Fig. 1 below).

Experimental studies of undrained two-dimensional froths [2] exhibit systematic deviations of threefold vertex angles from the force-balance angle of $2\pi/3$ [2]. Conversely, experiments done in the dry-froth limit have not shown measurable angle deviations [4]. The angle deviations reported for undrained froths have been previously explained by the combination of film curvature and large Plateau borders [12]. However, small angle deviations are *required*, even for dry froths, in order to create a net force on vertices to allow them to move against viscous drag and accommodate continuous bubble growth. In this paper, we use a force-based model (see Sec. II) that allows us to measure angle deviations. We find small local angle deviations for *dry* froths that depend on the side-number n in the same way as experimentally observed angle deviations of *undrained* froths [2].

Experimentally [13], four-sided and five-sided bubbles have been observed to annihilate directly through $T2_4$ and $T2_5$ processes, without any intervening $T1$ processes, consistent with theory [14]. However, previous numerical studies [6–10,15] have not clearly distinguished between four-sided and five-sided bubbles that directly annihilate at microscopic scales and those that shed sides through $T1$ processes at macroscopic scales before annihilating. There is a related controversy over whether *any* $T1$ events occur for macroscopic bubbles in the scaling regime [10,13], or whether all late-time $T1$ events are associated with microscopic side-shedding during bubble annihilation [16,17]. To resolve this

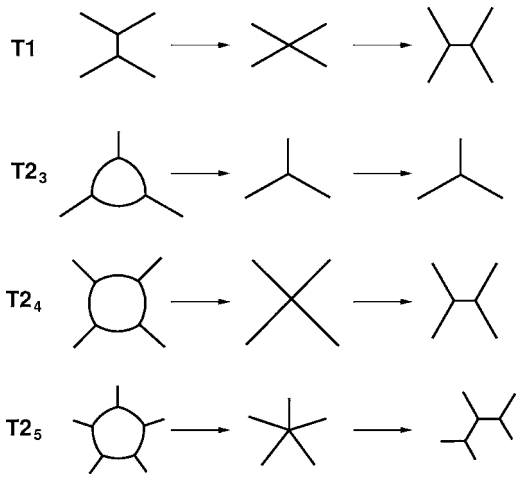

FIG. 1. Illustrations of the fast topological processes involved in froth evolution. From top to bottom are a side-switching $T1$ event, and three-, four-, and five-sided bubble deletions ($T2_3$, $T2_4$, and $T2_5$, respectively). From left to right are examples of the bubble walls and vertex positions before, during, and after the corresponding topological process. The details of resolution of $T2_4$ and $T2_5$ events will, in general, be determined by the forces acting along the bubble walls, as described in Sec. II.

*Electronic address: andrew.rutenberg@dal.ca

controversy, we precisely distinguish macroscopic and microscopic topological events. In the scaling regime of our model froth, we confirm the experimental observations of direct annihilation of four-sided and five-sided bubbles at microscopic scales. We also observe a significant rate of macroscopic $T1$ events in the scaling state.

A standard measure of the topological structure in 2D froths is the second moment of the side-distribution function, $\mu_2 \equiv \langle n^2 \rangle - \langle n \rangle^2$, where n is the number of walls of an individual bubble. Detailed froth models have recovered μ_2 values ranging from 1.2–1.6 [7–10] with reports of sensitive dependence of μ_2 on the details of $T2_4$ and $T2_5$ processes [8,9]. The frequently quoted experimental value of $\mu_2 = 1.4 \pm 0.1$ comes from an undrained froth experiment [2]. Measurements of μ_2 are bedeviled by long-lasting initial transients. In this study, we find $\mu_2 = 1.24 \pm 0.01$ and show that the transient after the initial μ_2 peak can last a decade in time. Our result is consistent with the late-time experimental results of undrained froths [2], and with previous numerical work on a locally equilibrated dry froth [10].

Computational model froths range from fast "topological" models that retain only bubble adjacency information (see, e.g., [8,15]), to "vertex" models that also include vertex positions but not bubble curvature [8,18], to "detailed" froth models that include vertex positions and uniform bubble curvatures [6,7,9,10] or even nonuniform bubble curvatures [19]. Each of these approaches trade off computational efficiency against structural detail in order to study different aspects of froths. However, detailed froth models are now capable of *precise* studies of the late-time scaling regime of a two-dimensional froth.

With a detailed force-resolved froth model (see Sec. II) that includes vertex positions and uniform wall curvatures, we precisely characterize the scaling state of two-dimensional dry froths. Starting with up to 10^4 bubbles, we reach the scaling state after long transients. In the scaling regime, we determine the second-moment of the side-number distribution μ_2 and the area growth-law amplitude $\langle A \rangle / (tD\sigma)$ (Sec. III A). We also characterize the angle deviations at bubble vertices, and find universal angle deviations associated with slow bubble coarsening (Sec. III B). Finally we find a significant number of macroscopic $T1$ events occurring in the scaling regime, and find that most bubbles annihilate as four-sided bubbles through $T2_4$ events (Sec. III C).

II. DETAILED FORCE-BASED FROTH MODEL

We implement a detailed force-based froth model with deterministic dynamics for both the slow evolution of bubble areas and for fast topological rearrangements. Froth coarsening is driven by gas diffusion between bubbles with a rate proportional to the diffusion constant, D, the full length of the intervening film, and the pressure difference across the film,

$$d\mathcal{N}/dt = D \oint \Delta P dl, \tag{2}$$

where we impose an ideal gas relationship $\mathcal{N} = PA$, where A is the bubble area and P is the bubble pressure. For locally equilibrated vertices and bubble walls, Eq. (2) exactly recovers von Neumann's law [11].

In a physical froth, vertices between bubble walls are associated with finite Plateau borders and will require a net applied force to be moved against viscous effects. Forces are applied along the three films meeting at the vertex, each with a constant magnitude equal to the surface tension σ of the film. A net force is applied, leading to vertex motion, if and only if some of the angles between adjoining films differ from $2\pi/3$. The vertex speeds will thereby be

$$\vec{v} = \gamma\sigma \sum_i \hat{\iota}, \tag{3}$$

where the $\hat{\iota}$ are unit vectors tangent to the films meeting at a vertex and γ is the vertex mobility, which we take to be constant.

While we assume that the internal relaxation of each bubble wall to a constant curvature is rapid enough to be ignored in the study of the scaling regime, for computational efficiency we allow for each film curvature, κ, to dynamically relax towards the local steady state by

$$d\kappa/dt = \Gamma(\Delta P - \kappa\sigma), \tag{4}$$

where Γ is the curvature mobility [20] and ΔP is the pressure difference between the two bubbles separated by the film. For any $\Gamma > 0$ our model is effectively in the high curvature mobility limit compared to the *natural* curvature dynamics [20] and indeed we find that curvatures quickly approach the equilibrated limit $\kappa = \Delta P/\sigma$ in the scaling regime.

The essence of both $T1$ and $T2$ processes is the temporary coalescence of two or more threefold vertices into an n-fold vertex, followed by the dissolution of that n-fold vertex. This all happens at microscopic length and time scales, determined in experimental systems by the Plateau border size. Our approach implements this phenomenology, though we choose computationally convenient microscopic lengthscales and rely on the universality of dry-froth structure to those scales. We enter into $T1$ topological processes when adjacent vertices approach within a microscopic distance, r_c, of each other, and into $T2$ processes when a bubble area decreases below $10r_c^2$. A finite r_c allows us to use a fixed time step, Δt [10]. For a $T1$ process, we temporarily replace two participating threefold vertices with one fourfold vertex at the midpoint, while, for $T2_n$ processes, we replace n threefold vertices with one n-fold vertex at the centroid of the deleting bubble. To resolve any n-fold vertex, we first determine the two adjacent films whose combined force upon the vertex is greatest, in the center-of-force frame. A short film of length r_c is placed between these two films and the other films of the vertex, oriented with the combined force, giving an $n-1$-fold vertex and a threefold vertex; this process is repeated until only threefold vertices remain. This approach reproduces the natural instability of fourfold and fivefold vertices [14], and follows the lowest energy (highest force) channel for resolving n-fold vertices. The entire topological process is implemented between time steps. Our results are not sensitive to r_c, as long as it is much smaller than the average bubble scale, or to the precise details of the placement or resolution of the n-fold vertex at scales of r_c.

The continuous evolution of vertices, curvatures, and bubble area is implemented with an Euler time discretization with time step $\Delta t=0.01$, supplemented with the dynamical rules for topological processes. Except where otherwise noted, we use $\sigma=1$, $\gamma=1$, $\Gamma=0.5$, $D=0.2$, and $r_c=0.01$. Our systems are initialized with up to $N_0=10^4$ bubbles with a random but periodic Voronoi construction. To control for finite-size effects, we have investigated different N_0 while keeping a fixed initial average bubble area and pressure, $A_0=10^3$ and $P_0=1$, respectively. We average at least 50 independent samples for $N_0=10^4$, and displayed error bars are statistical [21].

It is useful to compare our model to two other detailed froth models that have been studied in the scaling regime and that include both vertex positions and bubble curvatures.

Chae and Tabor [9] impose curvature equilibrium, i.e., $\Gamma\to\infty$, but have taken a length-dependent vertex mobility $\gamma\propto 1/\Sigma l_i$ where l_i are the lengths of the films adjoining the vertex [18]. At late times, as typical side lengths grow as $l\sim t^{1/2}$, they will have $\gamma\sim t^{-1/2}$. As discussed at the end of this paper, we expect their low mobility to lead to constant magnitude angle deviations in the scaling regime and to therefore affect other aspects of the scaling structure. Chae and Tabor allow all $T2_n$ processes, but impose various *ad hoc* side-shedding rules for resolving $T2_4$ and $T2_5$ processes, and find that μ_2 depends on which scheme is used [9].

Herdtle and Aref [10] build their model around an exact implementation of von Neumann's law, Eq. (1), and impose locally equilibrated vertex angles and film curvatures. In terms of our dynamics, they implement the γ, $\Gamma\to\infty$ limit in Eqs. (3) and (4), respectively. They only allow $T2_3$ bubble deletions, and resolve shrinking four-sided and five-sided bubbles very finely in time to catch all of the deterministic $T1$ side shedding that occurs at microscopic scales [10]. We believe that our force-based resolution of $T1$ and $T2_n$ events is equivalent to that of Herdtle and Aref [10] since the same film asymmetries that lead to side shedding at microscopic scales in their model will lead to vertex shedding from n-fold vertices in our model. While our finite vertex mobility does lead to nonzero angle deviations, they are too small to affect the structure in the scaling regime. We expect that our model should recover the same scaling state of the froth as Herdtle and Aref. However, their imposition of local equilibrium at all stages of froth evolution requires computational time of $O(N^{1.3})$ to execute each time step [10], where N is the number of bubbles, as opposed to $O(N)$ for our force-based algorithm. As a result, our algorithm allows larger froths to be studied in the scaling regime.

III. RESULTS

A. Scaling state

Two-dimensional soap froths exhibit dynamic scaling at late times. In the scaling state, the structural properties of the froth are time independent once appropriately adjusted for the shrinking number of bubbles $N(t)$ or growing average area per bubble $A(t)$. Topological structure such as the distribution function of the side number of individual bubbles becomes time independent even without scaling. Correlations in cellular systems, such as 2D froths, appear to be universal due to the strong separation in length scales and time scales between the continuous evolution of area and the fast $T1$ and $T2_n$ processes. Dry 2D froth experiments at various temperatures recover universal correlations [5], as do undrained experiments that vary the gas phase and hence diffusivity, D [2]. Our results are consistent with the existence of a universal scaling state at late times, though we have not systematically explored the parameter space of our froth model.

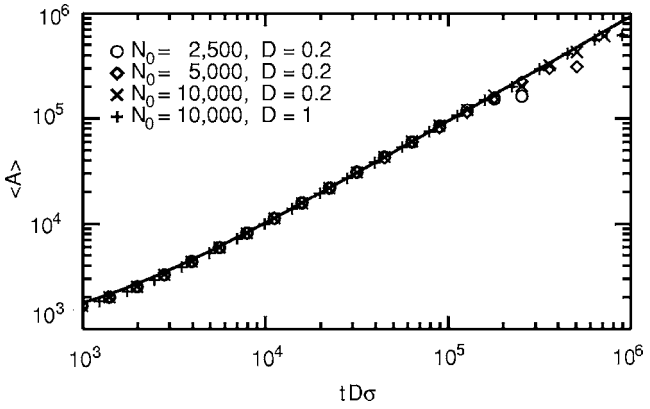

FIG. 2. The average bubble area of a coarsening froth, $\langle A\rangle$, vs the natural time variable, $\tilde{t}\equiv tD\sigma$. We see that linear growth is obeyed at late times, with a best-fit $\langle A\rangle=0.94^{\pm 0.01}(\tilde{t}-\tilde{t}_0)$ indicated by a solid line [21]. The amplitude is expected to universally apply to coarsening froths in their scaling state, with the effective time origin $\tilde{t}_0$ determined by initial conditions.

From von Neumann's law, we can directly see that $\langle A\rangle\sim t$ [5], and this is generally observed [11,17,22]. Since the froth evolution is driven by von Neumann's law [Eq. (1)], the natural time variable is

$$\tilde{t}\equiv tD\sigma, \tag{5}$$

and includes both the diffusivity and the surface tension, but not the curvature or vertex mobilities, Γ and γ, respectively [20]. As shown in Fig. 2, we recover the expected coarsening law for $\tilde{t}\gtrsim 10^4$, after initial transients. We see finite-size effects enter for $\tilde{t}\gtrsim 2\times 10^5$ and for $N_0=10^4$, roughly when the number of remaining bubbles drop below 100. We fit [21] the amplitude $\langle A\rangle/\tilde{t}=0.94\pm 0.01$ in Fig. 2, which we expect to be universal.

We next measure the surface energy of the froth, E, normalized by $E_{\rm hex}=N\sigma\sqrt{2\sqrt{3}A_0}$, the energy of a regular hexagonal froth with the same average bubble size, A_0 [9,10]. Our result [21], $E/E_{\rm hex}=0.938\pm 0.001$ is shown in Fig. 3 and is consistent with the best previous measurement (0.945 ± 0.010 [10]), though with higher precision.

Simulations of dry froths [7–10,23] have given values of the second moment of the distribution of the number of sides in a bubble, $\mu_2\equiv\langle n^2\rangle-\langle n\rangle^2$, that range between 1.2 and 1.6. As shown in Fig. 4, we observe [21] a constant, asymptotic value of $\mu_2=1.24\pm 0.01$. While broadly consistent with pre-

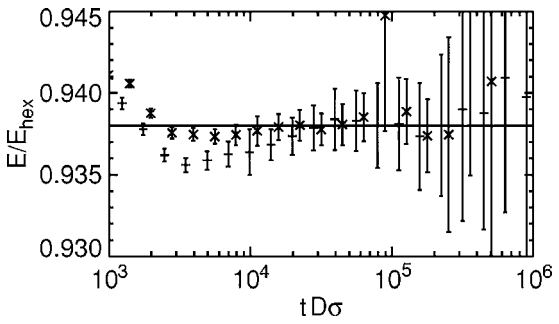

FIG. 3. Film energy of a coarsening froth, E, equal to the surface tension σ times the total film length, normalized by the energy of a uniform hexagonal froth $E_{\mathrm{hex}} \equiv N\sigma\sqrt{2\sqrt{3}A_0}$, with the same number of bubbles, N, and average bubble area, A_0, plotted vs $\tilde{t} = tD\sigma$. The asymptotic value in the scaling state is $E/E_{\mathrm{hex}} = 0.938 \pm 0.001$ [21] indicated by the horizontal line. The symbols "×" and "+" indicate data from $D=0.2$ and $D=1$, respectively, both with $N_0 = 10^4$.

vious values, we are closest to Herdtle and Aref [10], who found $\mu_2 \approx 1.2$.

We expect that $A/\tilde{t}$, E/E_{hex}, and μ_2 are universal measures of the scaling state, and the asymptotic agreement of these measures for two different values of D supports this. However, both the initial froth configuration and the particular dynamical parameters of the model will affect initial transients. By varying D, we can simulate the effects of using various gas-phase components, much as experimental studies have used either helium or air in their froths [2]. For larger D, we qualitatively reproduce a strong preasymptotic μ_2 peak in Fig. 4 that was seen experimentally [2]. The transient regime after that μ_2 peak lasts approximately *one decade* in time. In the best experimental determination of μ_2, the entire experiment lasted only one decade after the μ_2 peak [2], and the latest time data also recovered $\mu_2 \approx 1.2$.

B. Universal angle deviations

In a force-balanced steady state, the angles between the three adjacent films that form a vertex will all be $\theta_0 \equiv 2\pi/3$. Any deviations from θ_0 will result in a net force and motion of the vertex against viscous drag, as described by Eq. (3). Since most bubbles in the froth are continuously evolving in size, as approximately described by von Neumann's law, Eq. (1), their vertices must be continuously moving, necessitating nonzero angle deviations. We expect internal angles typically greater than θ_0 for growing bubbles ($n > 6$) and internal angles less than θ_0 for shrinking bubbles ($n < 6$).

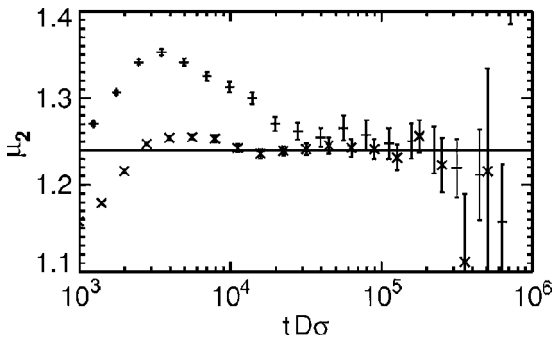

FIG. 4. The second moment of the side-number distribution, μ_2 vs $\tilde{t}$. We extract [21] an asymptotic value of $\mu_2 = 1.24 \pm 0.01$, indicated by a horizontal line. Significant transients are seen for the larger D data ("+"), including a distinctive preasymptotic peak. The symbols "×" and "+" indicate data from $D=0.2$ and $D=1$, respectively, both with $N_0 = 10^4$.

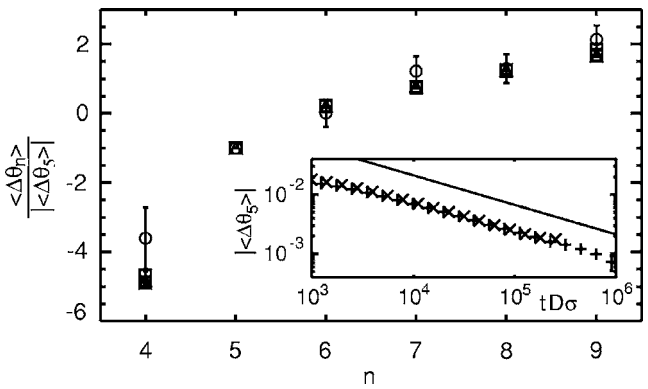

FIG. 5. Average angle deviations of n-sided bubbles scaled by the $n=5$ sided deviations, $\langle \Delta\theta_n \rangle / |\langle \Delta\theta_5 \rangle|$, vs n. The data are for $\tilde{t} = 27969$ (triangles and squares) and $\tilde{t} = 158217$ ("×" and "+") for $D=0.2$ and $D=1$, respectively. Also shown (circles) are the scaled data from experimental undrained froths [2], which illustrates the universality of the scaled angle deviations. Inset: time dependence of angle deviations of $n=5$ sided bubble vertices, $|\langle \Delta\theta_5 \rangle|$, scaled by γD^{-1} (see text) vs $\tilde{t} \equiv tD\sigma$. The solid line shows the expected $\tilde{t}^{-1/2}$ behavior. All data are with $N_0 = 10^4$.

In the scaling regime, the average bubble area grows as $\langle A \rangle \sim \tilde{t}$, with a characteristic length $L \equiv \sqrt{\langle A \rangle} \sim \sqrt{\tilde{t}}$ and vertex speed $v \sim dL/dt \sim \sigma D \tilde{t}^{-1/2}$. Small angle deviations will, according to Eq. (3), be proportional to vertex speeds divided by $\gamma\sigma$, so we expect $\langle |\Delta\theta| \rangle \sim D\gamma^{-1}\tilde{t}^{-1/2}$, where $\Delta\theta \equiv \theta - \theta_0$. As shown in the inset of Fig. 5, we observe this time dependence in the scaling regime. We also collapse the data for different D by scaling with γD^{-1}. Given this D dependence of $\langle |\Delta\theta| \rangle$, the previously observed D independence of $A/\tilde{t}$, E/E_{hex}, and μ_2 in the scaling regime indicate that the small observed angle deviations do not affect the froth structure. However, the scaled angle deviations can *characterize* the structure.

Different size Plateau borders in dry experimental froths will lead to different vertex mobilities, γ, and will in turn require different magnitude angle deviations for the same vertex speeds. If we scale out that magnitude, we should be left with universal angle deviations that reflect the universal froth structure. Indeed, in our data we find that angle deviations as a function of the number of bubble sides, scaled by the value for $n=5$, are time independent in the scaling regime for $3 < n < 10$ (see Fig. 5). Underlining this universality, the experimental data from undrained froths [2], indicated by circles in the figure, are consistent with our results within error bars.

Angle deviations have been previously explained as

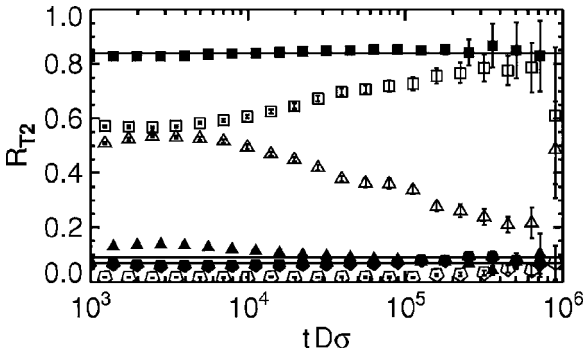

FIG. 6. The proportion of $T2_3$, $T2_4$, and $T2_5$ processes, for three-sided, four-sided, and five-sided bubble annihilation, denoted by triangles, squares, and pentagons, respectively, vs $\tilde{t}$. The filled symbols are for $D=0.2$ while the open symbols are for $D=1$, both with $N_0=10^4$. The number of sides are counted as the bubble area approaches microscopic scales, at $\ell \equiv \sqrt{r_c L(t)}$. The proportions approach constant values of $9^{\pm 2}\%$, $84^{\pm 2}\%$, and $7^{\pm 2}\%$, respectively, for $D=0.2$ [21], indicated by horizontal lines. Significant transients are apparent even at late times for $D=1$, though the trend is towards agreement with $D=0.2$.

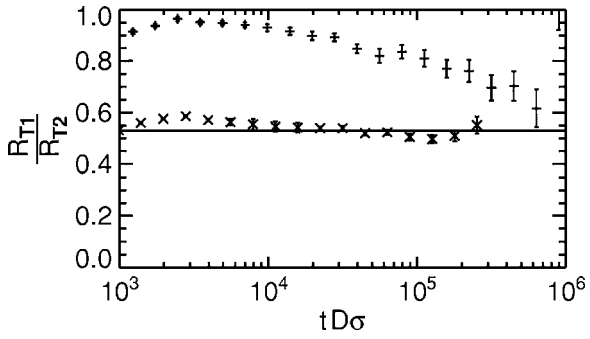

FIG. 7. The proportion R_{T1}/R_{T2} of macroscopic $T1$ events to microscopic $T2$ events, where only side shedding involving bubbles larger than $\ell \equiv \sqrt{r_c L(t)}$ are counted as $T1$ events. We find a ratio of $R_{T1}/R_{T2}=0.53\pm 0.05$ in the scaling regime [21], indicated by the horizontal line. Very long transients are found for $D=1$ ("+"), consistent with the previous figure.

arising from hidden angles due to the finite size of Plateau borders in combination with finite film curvatures [12]. However, our angle deviations are measured at the vertex center and do not include any explicit effects due to Plateau border size; they are independent of r_c. We believe that angle deviations measured experimentally are due to finite vertex mobilities, rather than Plateau border size *per se*. This distinction could be examined experimentally by varying the sample thickness, and hence effective vertex mobilities, while keeping the Plateau border size fixed.

Topological events also contribute to locally substantial angle deviations that are, however, subdominant in the scaling regime. We can qualitatively understand these deviations under the simplifying assumption that all angles equal θ_0 immediately before a topological event. As illustrated in Fig. 1, immediately after a $T1$ event, two of the six internal angles of the two separating vertices are $\pi/3$ rather than $2\pi/3$. Similarly, immediately after a $T2_4$ event two of the six internal angles about two vertices are $\pi/4$, and immediately after a $T2_5$ event, two of the nine internal angles around three vertices are $\pi/5$. These large angle deviations will last until a quasistatic configuration is reached by moving vertices a distance on the order of the bubble size, $L\sim t^{1/2}$. As shown in the next subsection, the rate of topological events is proportional to the rate of bubble annihilation, $R_{T2}\sim -dN/dt\sim t^{-2}$, so the average angle deviation due to topological events is expected to be only $\langle|\Delta\theta|\rangle_T\sim t^{-3/2}$, which is subdominant to the effects of continuous bubble evolution.

C. Topological processes

It is known that three-, four-, and five-sided bubbles can annihilate directly through $T2_3$, $T2_4$, and $T2_5$ processes, respectively [14]; however, it has not been clear what the relative rates of these processes are. To complicate the matter, while a three-sided bubble can only annihilate through a $T2_3$ process, a four- or five-sided bubble can shed sides through $T1$ processes at macroscopic scales and then annihilate through a $T2_3$ process. There have been qualitative reports that there are few if any $T1$ processes that are not associated with side shedding on the way to annihilation [13,17], and, indeed, simulations that only allow $T2_3$ processes that are self-consistent and yield results comparable to other models [10]. However, $T2_4$ and $T2_5$ processes have been reported experimentally [13].

What has been lacking is a clear definition of a $T1$ process as distinct from a $T2$ process. A natural distinction is between *macroscopic* $T1$ processes and *microscopic* $T2$ processes. $T1$ processes should be counted distinctly if they are associated *only* with macroscopic bubbles. Any side shedding that occurs at microscopic scales should simply be counted as the details of the associated $T2$ process. We have a natural microscopic scale that corresponds to the Plateau border size, r_c, while the average bubble size, $L\sim t^{1/2}$, provides an appropriate macroscopic scale. The geometric mean of these two lengths provides a natural division between microscopic and macroscopic, $\ell \equiv \sqrt{r_c L(t)}$. At late times, ℓ will be far from both microscopic and macroscopic scales. We count $T1$ events distinctly if all bubbles involved have areas larger than ℓ^2, and count $T2_n$ events if the bubble has n sides as it shrinks past the area ℓ^2. Scaling ℓ by a constant factor can significantly change the duration of initial transients, but it should not change results in the scaling regime.

We have measured the proportion of bubbles which vanish with three, four, and five sides, through the $T2_3$, $T2_4$, and $T2_5$ processes illustrated in Fig. 1. The proportions of these processes have not been reported in the literature, despite qualitative reports of $T2_4$ and $T2_5$ processes in undrained froths [13]. As shown in Fig. 6, these proportions are constant in the scaling regime, and have the values of $9^{\pm 2}\%$, $84^{\pm 2}\%$, and $7^{\pm 2}\%$ for $T2_3$, $T2_4$, and $T2_5$ processes, respectively. What is surprising is how few bubbles annihilate with three sides. This is qualitatively consistent with how few small three-sided bubbles are observed in froths in the scaling state; it also indicates how important $T2_4$ and $T2_5$ processes are in froth dynamics.

We have also measured the ratio of rates of macroscopic $T1$ to bubble annihilation $T2$ processes, R_{T1}/R_{T2}. This ratio

has been measured in simulations by Herdtle and Aref [10] to be 3/2, but they included microscopic side-shedding events so their result provides an upper bound to ours. As shown in Fig. 7, we find a ratio of $R_{T1}/R_{T2} \approx 0.53 \pm 0.05$. This indicates that macroscopic $T1$ events are significant even in late stages of froth coarsening.

IV. SUMMARY AND DISCUSSION

We have accurately characterized the scaling regime of a two-dimensional dry froth with natural force-resolved topological processes. We find values of $\mu_2 = 1.24 \pm 0.01$, $\langle A \rangle / \tilde{t} = 0.94 \pm 0.01$, and $E/E_{\mathrm{hex}} = 0.938 \pm 0.001$, independent of the gas diffusivity D. Our results for μ_2 and E/E_{hex} are consistent with previously measured values [10] though considerably more accurate, while our results for $\langle A \rangle / \tilde{t}$ have not been previously reported. These results are consistent with the hypothesis of a universal scaling state in two-dimensional froths, independent of the microscopic details of the model as long as natural topological processes are used [9].

We have shown that deviations from $2\pi/3$ vertex angles have a nonuniversal magnitude $\langle |\Delta\theta| \rangle \sim t^{-1/2}$ that is a consequence of the constant vertex mobility, γ. When scaled by the angle deviations for $n=5$ bubbles, the scaled angle deviations are time independent, independent of D, and agree quantitatively with experiment in Ref. [2], indicating their universality. This universality of the scaled angle deviations reflects the universality of the froth structure, as well as the robustness of the topological processes to the small and continuously decreasing angle deviations that remain in the scaling state.

The constant vertex mobility, γ, in our model is phenomenological; it was not derived from an underlying microscopic model of a froth. It leads to small and decreasing angle deviations in the scaling regime that asymptotically do not affect the scaling structure. Any detailed model with equilibrated vertex angles (see, e.g., [6,7,9,10,19]) would therefore be in the same dynamical universality class as our model, in this respect. Indeed, any model with characteristic forces that decay with time should be in the same "fast vertex" universality class as our model, since small angle deviations are proportional to the applied force. For example, the work of Bretherton [24] implies that the actual drag force f on vertices scales is $f \sim v^{2/3} \sim t^{-1/3}$, where the vertex speed $v \sim t^{-1/2}$, and so should lead to the same *scaled* angle deviations as our model. In contrast, the phenomenological mobility from vertex models (see Refs. [8,18,9]), $\gamma \sim 1/L \sim t^{-1/2}$, leads to *constant* magnitude angle deviations in the scaling regime since $\Delta\theta \sim f \sim v/\gamma$. Because constant magnitude angle deviations will bias the resolution of $T2_4$ and $T2_5$ processes, we expect *nonuniversal* structure (depending on the mobility) for these vertex models in the scaling regime.

Angle deviations have not been observed experimentally for dry froths [4], presumably because the vertex mobilities were so large in the dry froth limit that angle deviations were below the experimental resolution. Scaled angle deviations for undrained froths [2] agree with our results, supporting fast-vertex universality. While the time dependence of angle deviations was not reported [2], a direct comparison would be inappropriate without knowing the time dependence of the vertex sizes and hence of the effective mobilities.

We have also characterized the topological processes occurring in the scaling state. We make a clear distinction between $T2$ events occurring at microscopic scales, on the order of r_c and $T1$ events occurring at macroscopic scales on the order of $\sqrt{\langle A \rangle}$. We find that most annihilating bubbles have four sides ($84^{\pm 2}\%$) while relatively few have three ($9^{\pm 2}\%$) or five sides ($7^{\pm 2}\%$). We also characterize the ratio of side switching $T1$ events to bubble-annihilating $T2$ events and find a significant number of $T1$ events for macroscopic bubbles in the scaling state, $R_{T1}/R_{T2} = 0.53 \pm 0.05$. This is a significant result, since many topological froth models (e.g., [15]) neglect macroscopic $T1$ processes. This simplification appears to be unjustified. We expect significant effects in the scaling structure due to these $T1$ processes.

The precise agreement of our structural measurements with the results of Herdtle and Aref [10], indicates that our natural force-based resolution of $T2$ processes is consistent with their deterministic side shedding within $T2$ processes at microscopic scales. Our model appears to be in the same dynamical universality class as the model of Herdtle and Aref [10]. Since our model is local, its computational cost is $O(N)$ where N is the number of bubbles in the froth, which is significantly faster than their continuously equilibrated model [$O(N^{1.3})$] [10] particularly for the large froths ($N_0 \gtrsim 10^4$) needed to reach the scaling limit. Our force-based detailed froth model is simple, versatile, fast, and accurate.

Our curvature mobilities are deliberately fast [20], and we have imposed uniformly curved bubble walls. These approximations were necessary for computational efficiency, and common to previous computational studies of the scaling regime [6–10]. We believe that we are in the same dynamical universality class as coarsening experimental froths in the scaling state.

To affect the scaling state structure of the froth, dynamical features should significantly change either the asymptotic von Neumann's law or the resolution of topological processes in the scaling state. This becomes a significant issue for sheared froths [25] since $T1$ rates are constant under steady shear rates rather than decaying in frequency as in a coarsening froth. Following the argument of Sec. III B, we expect nonzero shear rates to lead to constant angle deviations in the steady state for any model with a finite vertex mobility, where the magnitude of the angle deviations will depend on the details of the vertex mobility. Since the effect of angle deviations on froth structure will depend on their magnitude, it will be important to get the vertex mobility right for precise models of sheared froths. The same can be said for bubble wall dynamics. Detailed "viscous froth" models (e.g., [19]), which relax the assumption of constant bubble wall curvature, may be necessary for the accurate study of sheared froths. We believe that finite and physically accurate vertex mobilities will also be needed for precise studies of sheared froths, to account for finite angle deviations in the steady state.

ACKNOWLEDGMENTS

We thank the National Science and Engineering Research Council of Canada for support. A.D.R. thanks Petro-Canada for additional support. Computer resources were provided by the Canadian Foundation for Innovation, by the Institute for Research in Materials at Dalhousie University, and also by the Advanced Computational Research Laboratory at the University of New Brunswick. We thank Michael Greenwood and Peter Cordes for initial coding and stimulating discussions.

[1] D. Weaire and S. Hutzler, *The Physics of Foams* (Oxford University Press, Oxford, 1999); J. Stavans, Rep. Prog. Phys. **56**, 733 (1993).
[2] J. Stavans and J. A. Glazier, Phys. Rev. Lett. **62**, 1318 (1989).
[3] D. J. Durian, D. A. Weitz, and D. J. Pine, Phys. Rev. A **44**, R7902 (1991).
[4] J. Stavans, Phys. Rev. A **42**, R5049 (1990).
[5] W. Y. Tam and K. Y. Szeto, Phys. Rev. E **53**, 877 (1996).
[6] D. Weaire and J. P. Kermode, Philos. Mag. B **48**, 245 (1983); J. P. Kermode and D. Weaire, Comput. Phys. Commun. **60**, 75 (1990).
[7] D. Weaire and H. Lei, Philos. Mag. Lett. **62**, 427 (1990).
[8] L. Neubert and M. Schreckenberg, Physica A **240**, 491 (1997).
[9] J. J. Chae and M. Tabor, Phys. Rev. E **55**, 598 (1997).
[10] T. Herdtle and H. Aref, J. Fluid Mech. **241**, 233 (1992).
[11] J. A. Glazier and D. Weaire, J. Phys.: Condens. Matter **4**, 1867 (1992).
[12] F. Bolton and D. Weaire, Philos. Mag. B **63**, 795 (1991); D. Weaire, Phys. Rev. Lett. **64**, 3202 (1990); A. V. Neimark and M. Vignes-Adler, Phys. Rev. E **51**, 788 (1995).
[13] J. A. Glazier, S. P. Gross, and J. Stavans, Phys. Rev. A **36**, 306 (1987).
[14] V. E. Fradkov, M. O. Magnasco, D. Udler, and D. Weaire, Philos. Mag. Lett. **67**, 203 (1993).
[15] B. Levitan and E. Domany, Europhys. Lett. **32**, 543 (1995); Phys. Rev. E **54**, 2766 (1996).
[16] J. Stavans, E. Domany, and D. Mukamel, Europhys. Lett. **15**, 479 (1991); H. Flyvbjerg, Phys. Rev. E **47**, 4037 (1993).
[17] J. Stavans, Physica A **194**, 307 (1993).
[18] K. Kawasaki, T. Nagai, and K. Nakashima, Philos. Mag. B **60**, 399 (1989); J. Stat. Phys. **57**, 759 (1989); T. Okuzono and K. Kawasaki, Phys. Rev. E **51**, 1246 (1995).
[19] N. Kern, D. Weaire, A. Martin, S. Hutzler, and S. J. Cox, Phys. Rev. E **70**, 041411 (2004).
[20] The natural curvature dynamics consistent with the microscopics for an isolated bubble is $v_\perp = \lambda^{-1}(\Delta P - \kappa\sigma)$ [11] where λ is an inverse mobility. This leads to curvature dynamics $\dot{\kappa} \propto \lambda^{-1}\kappa^2(\Delta P - \sigma\kappa)$, which implies that at late times, as $\kappa \to 0$, our dynamics, Eq. (4), is in the high mobility or $\lambda \to 0^+$ limit. We have used this limit in Eq. (1) [11].
[21] Fit values are extracted from an error-weighted average of the $D=0.2$ data for size $N_0 = 10^4$ systems in the interval $\tilde{t} \in [2 \times 10^4, 2 \times 10^5]$. Reported errors on fit values include estimated systematic errors due to initial transients and finite-size effects.
[22] J. A. Glazier and J. Stavans, Phys. Rev. A **40**, 7398 (1989).
[23] B. Levitan and E. Domany, Phys. Rev. E **54**, 2766 (1996).
[24] F. P. Bretherton, J. Fluid Mech. **10**, 16 (1961).
[25] G. Debregéas, H. Tabuteau, and J. M. di Meglio, Phys. Rev. Lett. **87**, 178305 (2001); A. D. Gopal and D. J. Durian, *ibid.* **75**, 2610 (1995).